Water Interfaces, Solvation, and Spectroscopy

Phillip L. Geissler

Department of Chemistry, University of California, Berkeley, California 94720, and Chemical Sciences Division, Lawrence Berkeley National Laboratory, Berkeley, California 94720; email: geissler@berkeley.edu

Annu. Rev. Phys. Chem. 2013. 64:317–37

First published online as a Review in Advance on January 16, 2013

The *Annual Review of Physical Chemistry* is online at physchem.annualreviews.org

This article's doi: 10.1146/annurev-physchem-040412-110153

Keywords

liquid water, interfaces, ion solvation, isosbestic behavior, vibrational spectroscopy

Abstract

Liquid water consistently expands our appreciation of the rich statistical mechanics that can emerge from simple molecular constituents. Here I review several interrelated areas of recent work on aqueous systems that aim to explore and explain this richness by revealing molecular arrangements, their thermodynamic origins, and the timescales on which they change. Vibrational spectroscopy of OH stretching features prominently in these discussions, with an emphasis on efforts to establish connections between spectroscopic signals and statistics of intermolecular structure. For bulk solutions, the results of these efforts largely verify and enrich existing physical pictures of hydrogen-bond network connectivity, dynamics, and response. For water at interfaces, such pictures are still emerging. As an important example I discuss the solvation of small ions at the air-water interface, whose surface propensities challenge a basic understanding of how aqueous fluctuations accommodate solutes in heterogeneous environments.

1. INTRODUCTION

Water is a famously unusual liquid. Its necessity for human survival and omnipresence in our natural environment attract a kind and degree of attention uncommon for subjects of chemical research. Physically, it differs in important ways from the simpler liquids of other common molecules such as CO_2 and N_2. In particular, forces of cohesion in water are highly directional so that intermolecular structure is not dominated by the well-understood effects of packing (1). Instead, strong but noncovalent hydrogen bonds stabilize open configurations, in which a given molecule is surrounded by only about four immediate neighbors on average (rather than the roughly 12 nearest neighbors of a dense fluid of similarly shaped hard objects).

This combination of fervent interest and microscopic complexity makes the physical chemistry of liquid water fertile ground for debate. Arguments over the most basic aspects of aqueous structure and dynamics routinely arise. The difficulty of unambiguously resolving such issues owes in part to the fundamentally disordered nature of the liquid state, which cannot be meaningfully described in terms of a single low-energy configuration. Intermolecular arrangements vary significantly in time and space; fluidity emerges from the fact that even the most stable structural motifs come and go. Theoretically, this prominence of fluctuations makes impractical the direct application of highly accurate quantum chemistry methods, which do not permit sampling extensive rearrangements of large numbers of molecules. Experimentally, fluctuations hinder drawing detailed conclusions from any probe that averages over the behavior of many molecules. Tools approaching both the indisputable realism of experiment and the complete detail of molecular simulation remain a long way off.

Despite the lack of authoritative methodology, there is broad, although not unanimous (2), consensus on the character of intermolecular structure in water. Extensive evidence from theory and simulation points to tetrahedral coordination as the dominant motif. At any particular instant, a great majority of molecules donate two hydrogen bonds and receive two in turn (3). In the immediate vicinity of a typical molecule, a representative configuration in this picture is not so different from that of the crystalline state of ice. Imperfections (e.g., distorted hydrogen bond angles) and defects (e.g., a molecule transiently accepting only one hydrogen bond), however, accumulate and disrupt crystalline order on scales much larger than a molecular diameter.

Recent computational work by Molinero & Moore (4) bolsters this structural view and underscores its shaping influence on the emergent properties of water's liquid state. Eschewing atomistic details, they explored a schematic molecular model whose energetics act only to encourage locally tetrahedral structure. Computer simulations of this monatomic water model (adapted from a model of liquid silicon due to Stillinger and Weber) recapitulate many nontrivial behaviors of the real liquid, accurately predicting several anomalous thermodynamic trends as well the pair distribution function and parameters such as surface tension. These results caution against the notion that more detailed empirical models (e.g., simple point charge models, transferable intermolecular potential models, and their many elaborations), which make predictions of similar accuracy, approximate detailed energetics of the real liquid in a systematically improvable way. Whether achieved through complicated interactions or through coarse-grained geometric preferences, these models appear to owe much of their success to stabilizing locally tetrahedral coordination.

With modern computing resources, these kinds of empirical models can be examined with great statistical accuracy, over long timescales, and in a variety of contexts [e.g., near surfaces or under confinement (5–7)]. Such studies have yielded an understanding of aqueous statistical mechanics much deeper than a simple appreciation of typical molecular arrangements. Most notably, it has been demonstrated that density and polarization fluctuations constitute normal modes of

liquid water in many circumstances. More precisely, in molecular simulations of empirical water models, these collective variables exhibit statistics that are Gaussian to a remarkable degree, in some cases even far from equilibrium (8). The number of molecules occupying a small probe volume, for instance, is Gaussian distributed many standard deviations from the mean (9), as is the electric field experienced by a small solute. This insight has motivated, or justified in hindsight, powerful linear response theories (10–12). Because their validity is not limited to small forces, perturbations as violent as inserting a solute or introducing an extended wall can be addressed in simple terms and with great success. The breakdown of these Gaussian descriptions often signals the emergence of dramatic physical changes. For example, the insertion of hydrophobic objects of sufficient size effectively induces a local phase transition, altering qualitatively the statistics of density fluctuations (13, 14).

SFG: sum frequency generation

Such insight from simulations is inherently limited by the realism of computationally tractable molecular models, which can never be fully established. Detailed input from experiment is therefore crucially important, but it remains profoundly challenging. Spectroscopic tools that enable the precise characterization of small molecules and clusters in the gas phase are much less directly informative when applied to the fluctuating molecular environment of a liquid. Rather than a discrete set of sharply peaked resonances that can be assigned to specific structures, liquid-phase spectra tend to feature broad, asymmetric lineshapes reflecting diverse ensembles of molecular arrangements. It can be tempting to reconstruct such spectra as linear combinations of idealized resonances, each notionally corresponding to a distinct class of related configurations; unfortunately, there is usually little basis for doing so.

Predicting and interpreting spectroscopic response of aqueous solutions demand a more statistical view. The frequency of a molecular vibration (e.g., stretching of an OH bond) is generally sensitive to its microscopic surroundings. The combined signal from many molecules therefore reports a reduced description of the probability distribution of corresponding intermolecular structures. It may do so, however, in a complicated way, folding in both dynamical information and variations in transition strength to yield low-dimensional and feature-meager lineshapes. Worse yet, coupling between vibrational coordinates of nearby molecules can obscure even the identity of normal modes absorbing and emitting radiation. Research over the past decade, involving close communication between experiment and theory, has significantly clarified this situation. Some complications have been minimized by judicious choices of experimental conditions. Others have been addressed by advancing the theory and simulation of spectroscopic observations. The first part of this review concerns developments in this latter area. I focus on approximate, but theoretically well-grounded, views of hydroxyl stretching lineshapes, which provide a sound basis for rationalizing spectroscopic shifts, e.g., resulting from changes in temperature or solvation of ions.

In addition to establishing connections between microscopic structure and spectroscopic signatures, the theoretical study of vibrational lineshapes has inspired new ways to analyze and understand the high-dimensional output of molecular simulations. Nonetheless, its primary role in the context of bulk aqueous solutions has been to affirm and refine perspectives already well developed from simulations. Later parts of this article concern interfacial aqueous systems, whose behavior is not yet well understood, even for empirical molecular models. In particular, I discuss recent work on the statistical mechanics of water in heterogeneous environments, focusing on the peculiar phenomenon of small ions adsorbing to the air-water interface. Finally, I end with a review of recent work on surface-sensitive spectroscopies, in particular sum frequency generation (SFG) and its promise for revealing aspects of interfacial physics that are proving difficult to understand even in simulation.

2. HYDROXYL STRETCHING LINESHAPES

The interaction of hydroxyl (OH) oscillators with light has proved to be a fruitful probe of structure and dynamics in hydrogen-bonding systems (15). Although considerably weaker than an OH covalent bond, OH $\cdots$ O hydrogen bonds in liquid water are quite potent, costing roughly $10k_BT$ to distort or break. Spectroscopically, this strength is manifested by an appreciable loosening of the corresponding OH covalent bond (16–18), whose stretching frequency decreases by nearly 10% when engaged in a typical hydrogen bond. If one could follow the evolution of a given oscillator's frequency ω over time, the resulting trajectory would report on the extent of its hydrogen bond distortions and exchanges as well as the timescales over which they occur. This notional measurement is in fact a caricature of a feasible but difficult experiment, which we return to below.

Tracking the evolution of a molecule's hydrogen-bonding environment through the frequency of light absorbed and emitted by its hydroxyl bonds is subject to several provisos. Foremost is the requirement that OH stretching acts as a distinct vibrational mode. Such isolation is not achieved in pure H_2O (ℓ). Even for a single water molecule, coupling between stretching of the two OH bonds produces symmetric and asymmetric stretches as normal modes. In the liquid, nearly degenerate stretches of a large number of nearby molecules are expected to participate in a given normal mode (whose composition furthermore changes over time) (19–25). The degree to which this delocalization hinders a simple interpretation of vibrational spectra cannot be overstated. It has become standard practice to circumvent this complication by studying dilute isotopic mixtures, featuring HOD as a dilute "solute" in a large excess of either H_2O or D_2O. Here one of the hydroxyl species (either OH stretching at 3,400 cm^{-1} or OD stretching at 2,500 cm^{-1}) is well separated in frequency from other vibrational motions in its immediate surroundings, thus providing a well-defined, spatially localized mode to query spectroscopically. Precisely how coupling among modes in the isotopically pure liquid influences vibrational lineshapes is certainly an interesting question, but as it can be avoided, I do not discuss it. My emphasis is not on the richness of vibrational spectroscopy itself, but instead on what can be meaningfully inferred about fluctuations in intermolecular arrangements. In all discussions of spectroscopy here, dilute isotopic mixtures are assumed.

For the same purpose of elucidating liquid structure and dynamics, this section focuses on isotropic Raman measurements, which permit several simplifications. I first sketch the theoretical development of Raman lineshapes, omitting many details and subtleties, primarily to point out the nature of approximations that lead ultimately to an uncomplicated physical picture. Time-dependent perturbation theory for radiation-matter interactions provides the standard starting point, relating the Raman lineshape $I(\omega)$ to a microscopic time-correlation function (26):

$$I(\omega) \sim \mathrm{Re} \int_{-\infty}^{\infty} dt\, e^{-i\omega t} \langle \alpha(0)\alpha(t) \rangle. \qquad (1)$$

Here α is the isotropic polarizability operator for a tagged oscillator, and angled brackets denote a thermal average. At this point we have in mind a fully quantum mechanical system, in which the oscillator and its entire molecular environment evolve according to the time-dependent Schrödinger equation. If we embrace the profound nonlinearity of interactions among a dense collection of water molecules (as is necessary to obtain anything other than a generic lineshape), then significant approximations are required to make any progress at all. Propagating the detailed quantum dynamics of a high-dimensional, nonlinear system is simply infeasible with current methods and computing resources.

A reasonable way forward, in which only a very small part of the system is treated quantum mechanically, has been forged over many decades (26–28). Particularly in the case of aqueous

systems, Skinner and coworkers (29–33) have pioneered the adaptation and elaboration of mixed quantum-classical approaches to make calculation of $I(\omega)$ tractable without sacrificing the molecular details underlying its most interesting features. Because there is no clean or rigorous way to combine quantum and classical dynamics, this approach involves several assumptions, for instance, that the classical environment is not capable of inducing transitions between the oscillator's quantized vibrational states. Instead, this bath only causes its vibrational energy levels to vary in time, giving rise to a time-dependent energy gap $\hbar\omega_{10}(t)$ between the ground and first vibrationally excited states. In its simplest form, this analysis yields for the polarizability correlation function

IR: infrared

$$\langle\alpha(0)\alpha(t)\rangle \sim \left\langle \exp\left[i \int_0^t dt' \, \omega_{10}(t') \right] \right\rangle. \quad (2)$$

Among the issues one ignores to arrive at Equation 2 are fluctuations in the magnitude of the transition polarizability (i.e., the off-diagonal elements of α in the basis set of unperturbed oscillator eigenstates). Quantum chemistry calculations support the neglect of such non-Condon effects in the Raman spectroscopy of water (34, 35). By contrast, for the case of infrared (IR) lineshapes, analogous variations in transition dipole appear to be substantial (34, 36, 37). The IR spectrum is also influenced by molecular rotations in ways that do not affect the isotropic Raman signal (34). Such complicating factors can be included in IR calculations, but they obscure the relationship between spectroscopic observables and liquid structure.

Equations 1 and 2 provide a straightforward route to computing Raman lineshapes from molecular simulations. For each configuration along an extended molecular dynamics trajectory, one can determine ω_{10} by solving the one-dimensional time-independent Schrödinger equation for the vibrational coordinate. Averaging over many such trajectories (or alternatively over time), one can then evaluate $I(\omega)$ numerically. This procedure has been applied with many models of water to estimate IR and Raman spectra (34, 35, 37–40). In many cases, attempts were made to improve realism by including additional details such as the phenomenological attenuation of the correlation function due to dissipation and transfer of vibrational energy. With such adornments, these approaches have successfully captured the positions and widths of measured vibrational spectra. Our approach (detailed in 41, 42) follows a different spirit, further reducing the complexity of spectroscopic formalism to examine the most basic connections between lineshapes and fluctuations in intermolecular structure.

Specifically, we consider the simplest approximation for frequency shifts of the hydroxyl stretch due to its aqueous environment. Expanding the oscillator-bath interaction to low order, exploiting the light mass of hydrogen atoms compared to oxygen atoms, and estimating vibrational energy levels within first-order perturbation theory, we obtain a simple Stark effect relationship

$$\omega_{10} = \omega_{10}^{(0)} + Q\mathcal{E}, \quad (3)$$

where $\mathcal{E}$ is the electric field exerted by the liquid on the vibrating proton in the direction of the OH bond. The parameters of this linear relationship between the excitation energy and electric field are the unperturbed oscillator frequency $\omega_{10}^{(0)}$ and the dipole change upon excitation, Q (within a factor of $\hbar$). It would be reasonable to assign $\omega_{10}^{(0)}$ as the OH stretching frequency of an HOD molecule in the gas phase, and Q could be computed for such an isolated molecule using high-level quantum chemistry methods. Other researchers have also recognized the dominant role of electrostatic interactions in driving frequency fluctuations (30, 40, 43), parameterizing expressions similar to Equation 3 (some including a term quadratic in $\mathcal{E}$ as well) by fitting quantum chemistry results for small water clusters. We instead treat $\omega_{10}^{(0)}$ and Q as empirical parameters, taking from the derivation of Equation 3 only the suggestion of a direct proportionality between $\mathcal{E}$ and frequency shift $\omega_{10} - \omega_{10}^{(0)}$. The results of Reference 38 provide notably compelling support for such a straightforward

connection. Although different approaches have employed different prescriptions for computing ω_{10}, there is general agreement that tracking the frequency of hydroxyl stretching in liquid water is essentially tantamount to following the local electric field it experiences. The notion that a polar probe's sensitivity to the liquid environment focuses attention on collective electrostatic variables resonates strongly with insight from solvation dynamics studies featuring much larger chromophores as reporters of aqueous fluctuations.

Our final approximation in this Raman lineshape calculation concerns the rate τ_c^{-1} at which fluctuations in ω_{10} decay, or equivalently the timescale τ_c for the reorganization of an oscillator's electrostatic environment. As emphasized by Kubo's lineshape theory (44), the transience of fluctuations in transition frequency away from its mean tends to narrow spectroscopic resonances. The degree of this motional narrowing is determined by the extent of frequency fluctuations $\Delta \equiv \sqrt{\langle(\omega_{10} - \langle\omega_{10}\rangle)^2\rangle}$ relative to their duration, as characterized by the magnitude of $\gamma \equiv \tau_c\Delta$. We assume γ to be very large, in effect ignoring the transience of variations in ω_{10}. In this limit of inhomogeneous broadening, spectral line widths are determined solely by the diversity of environments an oscillator samples. This approximation, similar to several others mentioned above, is a reasonable starting point but is not strictly justified for OH stretching in H_2O (ℓ). Based on predictions of molecular dynamics simulations and on the kinds of solvent motions one expects to modulate ω_{10}, the value of γ should not in fact be very large.

The net result of these approximations is an almost embarrassingly scrimpy prediction for the Raman lineshape. Performing the Fourier transform in Equation 1 (with the assumption that ω_{10} is independent of time), and exploiting the linear relationship between ω_{10} and $\mathcal{E}$, we obtain

$$I(\omega) \propto P(\mathcal{E}), \tag{4}$$

where $P(\mathcal{E})$ is the equilibrium electric field distribution and $\mathcal{E} = Q^{-1}(\omega - \omega_{10}^{(0)})$ is implicitly a function of frequency. I would argue that this approximate connection between spectral lineshapes and the thermal statistics of local electric field fluctuations provides the simplest interpretation of vibrational spectra that is rooted in physically motivated approximations.

What is remarkable about this stripped-down theory is how accurately it can capture measured lineshapes. The kind of agreement that has been achieved with more complicated approaches would not be impressive in this case—by tuning the parameters Q and $\omega_{10}^{(0)}$, one could engineer precisely the center and width of a calculated resonance. The correspondence between computed electric field distributions and experimental measurements, however, is much more detailed (42, 45). **Figure 1*a*** shows the prediction of Equation 4 for the Raman lineshape of HOD in D_2O (ℓ), evaluated using the SPC/E model of water, alongside the corresponding experimental measurement. The agreement is particularly striking when $I(\omega)$ is plotted on a logarithmic scale, emphasizing spectral features corresponding to the low-probability wings of $P(\mathcal{E})$. These results were obtained with a value of $\omega_{10}^{(0)}$ only modestly above the gas-phase stretching frequency.

An appealing aspect of the approximate theory I sketch above is that its predictions do not vary much from model to model. This robustness reflects the disproportionate contribution to a proton's electric field by its hydrogen-bonding partner (39, 41, 46, 47). Empirical water models capture the statistics of local hydrogen-bonding geometries almost by construction, as this basic structural feature is strongly constrained by X-ray scattering measurements (which are widely used in model parameterization). Such a dominant role for fluctuating hydrogen bond strength supports conventional wisdom that high-frequency and low-frequency extremes of the OH stretching lineshape correspond to atypically weak and atypically strong hydrogen bonds, respectively. The added value of our electric field–based perspective becomes clear below when we discuss spectral shifts due to the solvation of small anions.

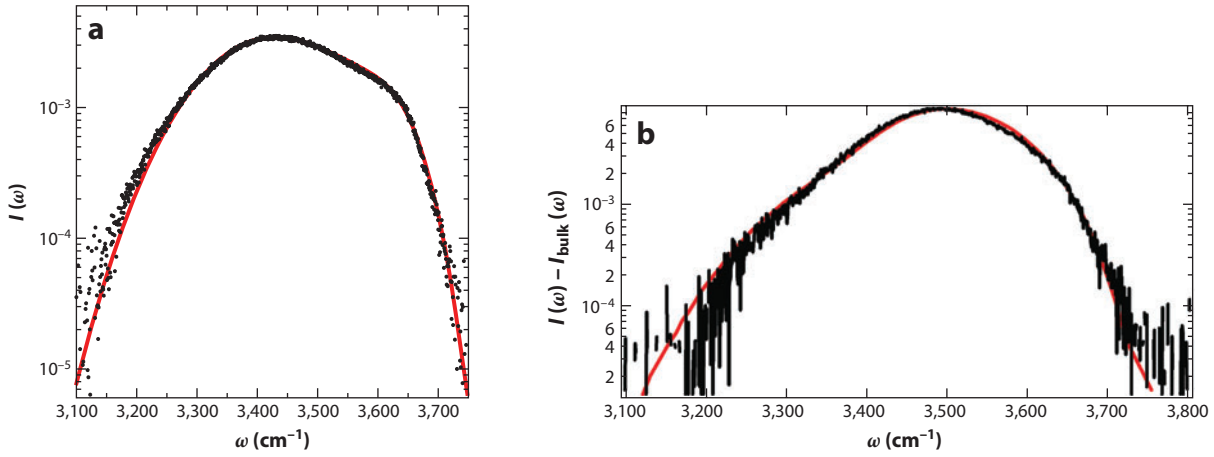

Figure 1

Raman spectra of dilute HOD in D_2O (ℓ), both for the neat liquid (*a*) and for a salt solution containing iodide anions (*b*). Experimental data are plotted in black. Red curves show theoretical predictions based on the simple theory of Equation 4 together with Monte Carlo simulations of the SPC/E model. In panel *b*, the signal I_{bulk} from water molecules not significantly affected by the ion's presence has been subtracted, as described in Reference 42.

By contrast, spectroscopic theories that account for truly dynamical effects (by relaxing the assumption of purely inhomogeneous broadening) yield results that can depend strongly on the choice of water model (37). Empirical models, after all, tend to differ more strongly in dynamics than in structure. What is especially puzzling is that dynamical "corrections" incorporated through the time dependence of $\omega_{10}(t)$ in Equation 2 typically do not improve agreement with experimental measurement, at least when freedom is allowed to adjust $\omega_{10}^{(0)}$ and Q. On the contrary, motional narrowing can mask features in the wings of $P(\mathcal{E})$ that are also present in measured spectra. **Figure 2** shows lineshapes computed from molecular dynamics simulations of the SPC/E model without assuming $\gamma \to \infty$. Even for the most favorable choices of Q, these correspond much less closely with measured Raman spectra. Unless the very close agreement between $P(\mathcal{E})$ and measured $I(\omega)$ is coincidental, it appears that the appropriate contribution of dynamics (and other factors we have neglected) in such empirical models is to establish an effective coupling Q between the frequency and electric field. How and why this renormalization might occur are very much open questions.

3. UNDERSTANDING SPECTRAL SHIFTS

This transparent framework for interpreting vibrational spectra has helped to resolve several debates about the significance of lineshape changes observed in experiments. I discuss two examples here. The first concerns shifts in frequency resulting from the introduction of dissolved ions. The second regards isosbestic behavior, i.e., the invariance of spectral intensity at a particular frequency to changes in thermodynamic parameters such as temperature. In both cases, the theory sketched above offers simple physical explanations for behavior that previously seemed at odds with a conventional understanding of aqueous structure and solvation.

3.1. Ion Solvation

Dielectric continuum theory (DCT) encodes the notion that coarse-grained polarization variables (e.g., the net dipole in a region of space comparable in size to a few water molecules) are, in

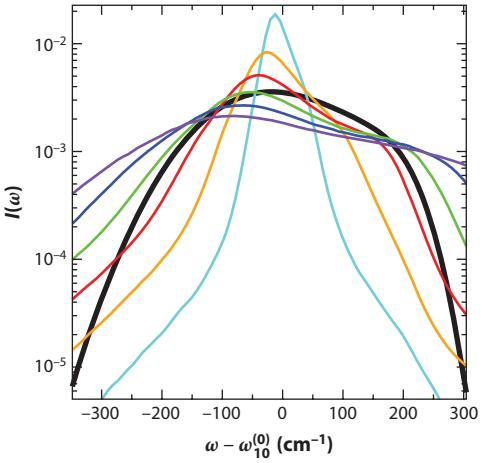

Figure 2

Raman lineshapes computed using Equations 1–3 without the assumption of purely inhomogeneous broadening (*colored curves*). The dynamics of ω_{10} were taken from molecular dynamics simulations of the SPC/E model. The result obtained from Equation 4, which neglects the dynamics of ω_{10} and matches experimental measurements quantitatively, is shown in black for comparison. Different colors indicate different values of the parameter Q determining the relationship between $\mathcal{E}$ and ω_{10}. In units of cm^{-1} /(V Å^{-1}), these values are $Q = 50$ (*cyan*), 100 (*orange*), 150 (*red*), 200 (*green*), 250 (*blue*), and 300 (*violet*).

appropriate linear combinations, the normal modes of a solvent's response to electrostatic perturbations (12, 48). The resulting linear response theory is supported in detail by results of molecular simulations (49). In this picture, a small ion dissolved in bulk water induces a reaction field in its environment, aligning solvent dipoles to produce highly favorable interaction energies. This dielectric response is generally opposed by interactions within the solvent, in DCT reducing the net solvation energy by a factor of two. In more molecular detail, a small anion achieves this polarization by accepting hydrogen bonds from several neighboring water molecules. Because most molecules in the undisturbed pure liquid donate hydrogen bonds using both hydroxyl groups, adopting this solvation structure requires breaking a number of OH $\cdots$ O hydrogen bonds.

The influence of dissolved salts on OH stretching spectra has been inferred to tell a rather different story, in particular for the solvation of anions. The Raman OH stretching band shifts to slightly higher frequencies when Cl^- is introduced at low concentration (42, 50–54). This effect is more pronounced for Br^- and stronger still for I^-. Based on the association of high frequencies with weak OH $\cdots$ O hydrogen bonds, investigators inferred that these halide ions are "structure breakers," which, in addition to seizing hydrogen bond donors for their direct coordination, distort solvent hydrogen bonds well into their surroundings (53–55). Ions causing shifts to lower frequencies ("structure makers") have been correspondingly imagined to enhance the strength of solvent hydrogen bonds.

Alternative explanations for these spectroscopic changes, which do not require such notions of structure making and structure breaking, are immediately apparent from the simplified lineshape theory of Equation 4. Hydroxyl groups engaged in hydrogen bonds with an anion sample a significantly different electrostatic environment than those associating with other water molecules. Their close approach to a very small ion should result in especially strong electric fields. These solute-generated fields attenuate, however, as ion size increases. In simulations of Br^- (aq) and I^- (aq), solvating protons experience fields weaker on average than in the pure liquid (42). According to Equation 3, these electric field trends translate directly into hydroxyl frequency shifts. The

DCT: dielectric continuum theory

resulting predicted lineshape changes, with an added population of high-frequency oscillators, match precisely the directions of observed shifts. In fact the agreement is more than qualitative, as illustrated by the difference spectrum (i.e., the Raman intensity above that expected for bulk water molecules unaffected by the solute's presence) in **Figure 1*b***. Computed and measured lineshapes correspond closely, even when viewed on a logarithmic scale. These calculations did not involve adjustable parameters, as Q and $\omega_{10}^{(0)}$ were fixed at values determined to be optimal for the pure solvent.

Ion-induced changes in vibrational spectra further emphasize the primary sensitivity of the OH stretching frequency to very local features of the oscillator's environment. Calculated difference spectra for halide ions are strongly dominated by directly coordinating hydroxyl groups, which reside only a few angstroms away from and are oriented strongly toward the solute. Monovalent cations, which lack such directly interacting hydroxyl groups, hardly influence electric field statistics (and measured vibrational lineshapes). Ion solvation certainly does affect liquid structure beyond this immediate environment but in ways that local electric fields do not distinctly manifest. For example, by accepting several hydrogen bonds and donating none, halide ions substantially alter the connectivity of water's hydrogen bond network over distances of several molecular diameters. This topological disruption is resolved, however, without noticeably compromising the geometry or energetics of individual OH $\cdots$ O bonds.

Given the crudeness of approximations underlying Equation 4, and the schematic nature of molecular mechanics models we have used to evaluate it, the quantitative agreement shown in **Figure 1** is quite surprising, especially in the case of salt solutions. Interactions between halides and coordinating water molecules not only are strong but are also believed to involve nonnegligible charge transfer. Empirically, the observed success encourages exploring the use of Equation 4 in a variety of physical contexts. Indeed, similar expressions and computational schemes have recently been implemented for biomolecular systems. Ultimately, however, it is important to understand why this set of approximations works so well (and why reasonable efforts to improve upon them are often counterproductive).

3.2. Isosbestic Behavior

Implications of Equation 4 for the temperature dependence of vibrational spectra are also informative. Electric field distributions determined from simulation reflect the broad and continuous diversity of local hydrogen-bonding geometries, ranging from low-energy, ice-like arrangements to highly distorted configurations several $k_B T$ higher in energy. Increasing temperature of course shifts statistical weight toward the higher-energy portion of this ensemble. The predicted OH stretching lineshape thus shifts to higher frequencies, as is also observed in experiment. In other words, upon heating, $I(\omega)$ and $P(\mathcal{E})$ both decrease at low frequencies and increase at high frequencies. At a particular intermediate value of frequency (an isosbestic point), intensity is approximately constant with temperature, varying little over the entire range of stability of the liquid state at ambient pressure (0–100°C).

Similar to ion-induced shifts in vibrational lineshapes, the isosbestic behavior of $I(\omega)$ has motivated unconventional views of microscopic structure and response in liquid water. Here a resemblance to spectroscopic trends in simpler systems could appear to support a discrete view of liquid fluctuations, perhaps implying a prominent role for broken hydrogen bonds. A dilute mixture of two interconverting species exhibits an absorption lineshape $A(\omega) = c_1 a_1(\omega) + c_2 a_2(\omega)$ that linearly combines the intrinsic absorptivities $a_1(\omega)$ and $a_2(\omega)$ of the individual components. Changing the relative proportions of the two species (e.g., by raising temperature) changes the coefficients c_1 and c_2 of this linear combination. As a result, spectroscopic intensity changes at all

frequencies except where $a_1(\omega^*) = a_2(\omega^*)$, giving rise to an isosbestic frequency ω^*. Analogous phenomenology in the Raman and IR spectra of liquid water inspired conjectures that hydrogen bond geometries interconvert between two distinct states (56–59).

This interpretation of bistability is not supported by molecular simulations, which rapidly explore a continuous ensemble of intermolecular arrangements characterized by primarily tetrahedral coordination. That electric field distributions determined from simulation also feature an isosbestic point suggests that two-state interconversion is not a unique source of temperature-invariant spectral intensity. Indeed, once a connection between $I(\omega)$ and $P(\mathcal{E})$ has been recognized, the statistical mechanics of equilibrium distributions provides a simple alternative explanation (45, 60). Differentiating $P(\mathcal{E})$ with respect to inverse temperature $\beta = 1/k_B T$ in the canonical ensemble, one obtains

$$-\frac{\partial \ln P}{\partial \beta} = \langle U \rangle_{\mathcal{E}} - \langle U \rangle, \tag{5}$$

where $\langle U \rangle_{\mathcal{E}}$ denotes the average energy of configurations sharing a given value of $\mathcal{E}$ (for a particular OH bond). The right-hand side of Equation 5 is mathematically guaranteed to vanish at some electric field value $\mathcal{E}^*$. Over a sufficiently small range ΔT of temperature, $P(\mathcal{E}^*)$ must therefore be constant to a good approximation, giving the appearance of isosbestic behavior. Assuming that a relatively small number of degrees of freedom control fluctuations in $\mathcal{E}$, Reference 60 presents a general argument that this range is limited only by the condition that $(\Delta T/T)^2$ be modestly smaller than 1. The observation that $I(\omega^*) \approx$ const from 0 to 100°C, corresponding to $(\Delta T/T)^2 \approx 0.1$, need not signify anything more than unremarkable thermodynamic changes in a continuous equilibrium distribution. This reasoning applies generally to inhomogeneously broadened spectra: In aqueous solutions, one should not be surprised by isosbestic behavior extending all the way from freezing to boiling of the solvent.

4. TWO-DIMENSIONAL INFRARED SPECTROSCOPY AND HYDROGEN BOND DYNAMICS

As described above, conventional IR and Raman spectra of liquid water offer a glimpse of the static distribution of electrostatic environments molecules explore. Sophisticated multidimensional vibrational spectroscopies pioneered over the past decade provide in principle a much richer, dynamical view (61–68). In effect, these experiments tag at a given moment a subensemble of hydroxyl groups sharing the same transient frequency and then follow their evolution over an ensuing 1–2 ps. During this time, an initially nonequilibrium distribution of intermolecular structures relaxes as OH oscillators randomly explore new environments. This idealization of a two-dimensional (2D) IR experiment would yield a time-dependent conditional probability $P(\omega(t)|\omega(0))$, i.e., the probability that an oscillator with initial frequency $\omega(0)$ evolves to frequency $\omega(t)$ after a time t. According to Equation 3, it thus characterizes in detail the timescales over which a water molecule's electrostatic environment changes.

For several technical reasons, a real 2D IR signal cannot provide quite such detailed information. (For one thing, the assumption of purely inhomogeneous broadening that allows a straightforward probabilistic interpretation is difficult to justify for an explicitly dynamical measurement.) But appropriate semiclassical response functions can be formulated—generalizations of Equation 2 embracing the dynamics of frequency fluctuations during three distinct time periods, each punctuated by an interaction with the radiation field—and evaluated using computer simulations (46, 61, 69–72). Agreement between theory and experiment in this case is not as precise as what has generally been achieved for conventional IR and Raman spectra (and not nearly

as compelling as the correspondence shown in **Figure 1**). Nonetheless, some basic implications of these measurements for hydrogen bond dynamics are clear. In particular, oscillators with initially weak hydrogen bonds [i.e., those with especially weak electric fields $|\mathcal{E}(\omega(0))| < |\langle\mathcal{E}\rangle|$ and $\omega(0) > \langle\omega_{10}\rangle$] relax rapidly toward $\langle\omega_{10}\rangle$, returning to more typical environments within 100–200 fs (66). The typical persistence time of these species is thus comparable with the fastest timescales of pertinent basic molecular motions (e.g., a few librational periods).

These results indicate that truly broken hydrogen bonds, which persist for a meaningful time before the OH group finds a willing acceptor, are exceedingly rare in bulk liquid water. The vast majority of high-frequency excursions either reflect transient fluctuations about a stable hydrogen bond or else represent transition states in the course of switching from one acceptor to another. Molecular simulations strongly support this interpretation, indicating that hydroxyl groups almost always reside within the basin of attraction of a stable hydrogen bond. Quenching representative configurations to nearby minima of the potential energy surface, or averaging over short time intervals (73), makes this fact especially clear. Given the strength of OH $\cdots$ O attraction relative to $k_B T$, this conclusion is a comforting resolution to decades-old debates regarding the stability and prevalence of broken hydrogen bonds.

5. FLUCTUATIONS AND RESPONSE AT THE AIR-WATER INTERFACE

Although rare in bulk liquid water, broken hydrogen bonds are a defining feature of the liquid's boundary. Simulations suggest that water's hydrogen bond network is sufficiently flexible to deform around excluded volumes on the subnanometer scale. More spatially extended constraints, such as those posed by a large hydrophobe or an interface with vapor, necessitate breaking hydrogen bonds (13, 74). These unsatisfied intermolecular attractions clearly underlie the substantial surface tension of air-water and oil-water interfaces. The ways they shape microscopic fluctuations and response, however, remain subjects of active research.

Statistics of the electric field variable $\mathcal{E}$ paint an interesting picture of such interfacial environments. **Figure 3** shows distributions $P(\mathcal{E}; z)$ resolved by the height z of an OH group relative to the mean interfacial position $\bar{z}_{\text{int}}$, determined from simulation. As $z \to \bar{z}_{\text{int}}$ from the liquid side, a new feature emerges in $P(\mathcal{E}; z)$ at low $|\mathcal{E}|$, corresponding to free OH groups that lack a hydrogen bond acceptor, an unambiguous signature of reduced connectivity at the interface. Strikingly, away from this extreme wing of the distribution, the shape of $P(\mathcal{E}; z)$ hardly changes with z. By this measure, intact hydrogen bonds near the liquid's boundary differ little from those in bulk. Just as for anion solvation in bulk aqueous solution, large perturbations to the connectivity of water's hydrogen bond network can be tolerated without appreciably modifying the character of individual bonds.

Molecular orientations at the air-water interface follow a similar pattern: Free OH groups in computer simulations are strongly oriented relative to the interface (pointing away from the liquid), whereas those engaged in hydrogen bonds show only a very weak average projection onto the surface normal (75). This average orientation of hydrogen-bonded OH groups is so weak, in fact, that its sign depends on seemingly arbitrary simulation details (76). In particular, for the periodic slab geometry of most interfacial simulations, calculating many surface properties requires assigning each molecule to one of the two opposing interfaces, which can be done in many different ways. (With other boundary conditions, the issue would arise in some other form.) This ambiguity has significant consequences for computing surface-sensitive spectroscopic signals, as described below.

The influence of interfacial constraints on solvation is more dramatic, especially in the case of small charged solutes (77–79). That density and polarization fluctuations serve as statistical

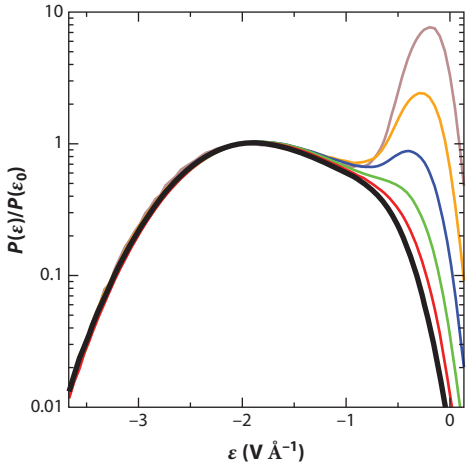

Figure 3

Probability distributions of the electric field variable $\mathcal{E}$ for hydroxyl groups in bulk water (*black*) and near an interface with vapor (*colors*). To emphasize similarity within the high-$|\mathcal{E}|$ subensemble of hydrogen-bonded species, all curves are scaled to have the same value at a reference frequency $\mathcal{E}_0 \approx -2\,\mathrm{V\,Å^{-1}}$. The topmost (*brown*) curve corresponds to OH groups roughly 1–2 Å above the mean interface height $\bar{z}_{\mathrm{int}}$; the next highest curve (*orange*) corresponds to OH groups roughly 0–1 Å above $\bar{z}_{\mathrm{int}}$; and so on. Readers are referred to Reference 76 for simulation details.

normal modes of bulk water motivates several expectations for ion solvation at the air-water interface. Most simply, as a charged solute leaves the solution phase and enters a low-dielectric environment, it must sacrifice the favorable energy of polarizing its aqueous surroundings. Indeed, according to textbook DCT calculations, a point charge in a high-dielectric phase is repelled from a flat interface with vacuum, through a force equivalent to a nearly identical image charge in the gas phase (80–82). The scale of dielectric solvation energies, $\sim 100\,k_{\mathrm{B}}T$ in the case of I^- (aq), suggests that this consequence of waning reaction fields will largely determine the spatial distribution of dilute dissolved ions, which should be strongly depleted at the interface relative to bulk solution.

The contribution of solvent density response to the excluded volume constraints imposed by a solute generally opposes solvation. In the case of water, this contribution is primarily entropic, reflecting decreased freedom in hydrogen bond network arrangements near a microscopic inhomogeneity. The thermodynamic bias toward removing a small solute from the liquid can be substantial, amounting to $\sim 10\,k_{\mathrm{B}}T$ for an iodide-sized cavity (13, 83, 84), but it fails to rival dielectric solvation energies. Nonetheless, as a small ion leaves solution, one expects the system to recover a modest entropy.

Remarkably, experiments and simulations indicate that each of these basic expectations can be violated: Charged solutes comparable in size to a solvent molecule [e.g., I^- (aq)] can be more concentrated at the interface than in bulk (77–79), can be driven to the surface by favorable energies of adsorption (85, 86), and can face entropies opposing adsorption that compare in scale to energetic driving forces (85, 86). This broadly counterintuitive behavior is general, occurring even in idealized models of polar fluids. It can be influenced by details absent in the models discussed here [e.g., polarizability of the electron distributions of solute and solvent molecules (87, 88)], but such complications are accessory in my view to the most intriguing aspects of this ion adsorption phenomenon.

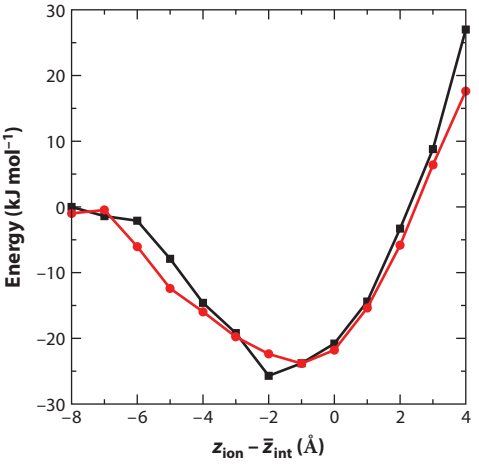

Figure 4

Average energy of a simulated liquid slab containing one fractionally charged, iodide-sized anion, as a function of the ion's height relative to the mean interface. Values obtained directly from simulation are shown in black. Values determined from the local approximation of Equation 6 are shown in red. Readers are referred to Reference 86 for simulation details.

The need for a new physical picture of interfacial solvation is underscored in simulations by breakdowns in simple statistics of density and polarization variables, on which approaches such as DCT are based. That density should exhibit non-Gaussian fluctuations is not at all surprising—the very existence of a stable interface arises from thermodynamic bistability underlying the liquid-vapor phase transition. Viewed another way, a microscopic probe volume near the fluctuating interface will sometimes be occupied by liquid and sometimes not, yielding bimodal distributions of local density. It is less obvious that the electrostatic fluctuations shaping ion solvation will become significantly more complex near the interface (89). Variations in surface topography over time, however, amount to fluctuating boundary conditions for dielectric response. Given the rich sensitivity of electrostatic Green's functions to boundary shape (80, 90), the emergence of nonlinear restoring forces for solvent polarization might be expected.

We have recently shown that negative adsorption energies can be understood in simple terms that expose important shortcomings of conventional DCT approaches (86). Specifically, our simulations suggest that the average energy $\langle U(z_{ion})\rangle$, as a function of ion height z_{ion}, can be accurately decomposed into a few spatially local contributions. Assigning a constant energy ϵ_{coord} to each solvent molecule directly coordinating the ion, an energy ϵ_{surf} to (noncoordinating) molecules near the liquid's surface, and finally an energy ϵ_{bulk} to molecules well away from both solute and surface, we find that

$$U_{local}(z_{ion}) \equiv (\epsilon_{coord} - \epsilon_{bulk})n_{coord}(z_{ion}) + (\epsilon_{surf} - \epsilon_{bulk})n_{surf}(z_{ion}) + \text{const} \qquad (6)$$

closely approximates the true average energy (see **Figure 4**). Here n_{coord} and n_{surf} are the average number of water molecules in coordination and surface environments, respectively, which change as the solute breaches the interface.

The first term in Equation 6 captures in molecular terms the physical effects discussed above in the context of DCT: n_{coord} decreases as an ion approaches the surface, shedding its solvation layers and thus sacrificing a favorable energy $(\epsilon_{coord} - \epsilon_{bulk})$ per coordinating molecule. The second term in Equation 6 describes a distinct aspect of surface energetics, one that is straightforward

to understand but is missing in DCT: By occupying volume in the interfacial region, a solute reduces n_{surf}, effectively decreasing the contact area between the liquid and vapor and lessening the energetic cost of $(\epsilon_{surf} - \epsilon_{bulk})$ per molecule at the liquid's boundary. In a language specific to aqueous systems, anions at the interface can scavenge previously unsatisfied hydrogen bond donors, without having to break OH $\cdots$ O bonds, as would be required in bulk. Similar forces are at play in the solvation of positively charged ions at the air-water interface. For reasons that are not yet well understood, their net effect in the case of cations is less conducive to adsorption (79).

The entropy S of interacting high-dimensional systems is much more difficult to parse. We have proposed that the observed minimum in $S(z_{ion})$ is associated with the same fluctuations that complicate statistics of density and polarization at the interface, namely, undulations of the liquid's boundary. These topographical fluctuations, whose long-wavelength components are known as capillary waves (91), persist down to molecular scales, at which they are unquestionably sensitive to an ion's presence. Simulations indicate that an ion with high surface propensity, when held at $z_{ion} = \bar{z}_{int}$, indeed tends to locally pin the interface (86). The consequent dampening of height fluctuations should significantly reduce the entropy of capillary wave-like modes. Such a mechanism is difficult to unambiguously demonstrate from detailed molecular models. It is supported, however, by more schematic lattice gas-like models that lack any other source of entropy (92). Because these lattice descriptions also capture the surface energy contributions underlying the minimum in $\langle U(z_{ion})\rangle$, they offer a promising framework for properly adapting DCT to fluctuating interfacial environments.

6. SURFACE-SENSITIVE VIBRATIONAL SPECTROSCOPY

The spectroscopic methods described above do not report on interfaces in macroscopic systems. In an aqueous sample at liquid-vapor coexistence, the fraction of water molecules that are sensitive to the phase boundary is negligibly small. Nonlinear measurements have been devised, however, that focus attention on such heterogeneous regions. Vibrational SFG, developed by Shen and coworkers (93), has become a particularly popular tool for studying liquid interfaces (94, 95). To the extent that a probe molecule can be represented as a point dipole, the SFG response is forbidden in the bulk environment by symmetry. From a theoretical perspective, the price of this clever way to isolate interfacial signals is that observable quantities are even more remote from the microscopic structural properties of interest.

SFG spectra for the air-water interface exhibit a pronounced peak at high OH stretching frequencies that are essentially unshifted from the gas-phase value. There is little doubt that this feature corresponds to the population of free OH groups described above. Almost every other aspect of the SFG spectrum in the hydroxyl stretching frequency range remains a subject of debate (96–98).

Simulation-based strategies for computing SFG spectra were pioneered by Morita & Hynes (99, 100). Their time-correlation function expressions for the dipole-order SFG susceptibility $\chi^{(D)}_{SFG}(\omega)$ were subsequently used to develop lineshape theories closely akin to Equation 2 (101, 102). The principal added complexity is the appearance of molecular orientation vectors, which highlight the danger of interpreting the SFG response as if it were a simple absorbance. Peaks in the intensity $|\chi_{SFG}(\omega)|^2$ measured in many experiments can arise, for example, from changes in the sign of Im $\chi_{SFG}(\omega)$, which clearly do not signify the existence of distinct structural populations. Phase-sensitive measurements, which resolve Im $\chi_{SFG}(\omega)$ itself (103), constitute an important step toward a meaningful interpretation of the SFG response.

The same set of approximations sketched above in the context of Raman spectroscopy can be followed to greatly simplify expressions for $\chi^{(D)}_{SFG}(\omega)$. They yield a susceptibility that linearly

combines several orientational averages, multiplied by the electric field distribution $P(\mathcal{E})$ (76). The behavior of these averages is mostly captured by the simplest such quantity, $\langle u_z \rangle_{\mathcal{E}}$. Here $\hat{\mathbf{u}}$ is a unit vector pointing along the OH bond, the subscript z indicates projection onto the surface normal, and the subscript $\mathcal{E}$ on angled brackets denotes a conditional average over oscillators with the same instantaneous value of the field $\mathcal{E}$. This result suggests that SFG is unlikely to reveal any surprising structural features of hydrogen-bonded OH groups at the neat air-water interface: These oscillators differ little in their electric field statistics from those in the bulk liquid, and their orientational bias is weak.

A stripped-down theoretical approach also lays bare a troubling issue that plagues all computational approaches to SFG reported to date (76, 104). Simply put, the dipole-order susceptibility $\chi_{\mathrm{SFG}}^{(\mathrm{D})}(\omega)$ is not a well-defined observable quantity. Quadrupole-order contributions $\chi_{\mathrm{SFG}}^{(\mathrm{Q})}(\omega)$ to SFG are not symmetry forbidden in bulk (105); as a result, they are effectively promoted one order higher in the molecular multipole expansion. There are thus no formal grounds for considering $\chi_{\mathrm{SFG}}^{(\mathrm{D})}$ independent of $\chi_{\mathrm{SFG}}^{(\mathrm{Q})}$; only their sum is physically meaningful.

The inseparability of dipole- and quadrupole-order SFG responses is highlighted by the ambiguous nature of orientational averages evaluated in liquid slab simulations. As mentioned above, the values of such averages depend on one's arbitrary convention for dividing the system into two distinct interfacial regions. Indeed, equally reasonable conventions can yield quite different predictions for SFG lineshapes. Quadrupole-order contributions suffer from a parallel issue, rooted in the fundamental ambiguity of defining the quadrupole moment of a charge distribution with nonvanishing net dipole. The sum $\chi_{\mathrm{SFG}}^{(\mathrm{D})} + \chi_{\mathrm{SFG}}^{(\mathrm{Q})}$ is immune to such problems, so long as conventions are applied consistently to both $\chi_{\mathrm{SFG}}^{(\mathrm{D})}$ and $\chi_{\mathrm{SFG}}^{(\mathrm{Q})}$. Simulation results for $\chi_{\mathrm{SFG}}^{(\mathrm{Q})}$ have not yet been reported, although the basic formalism has been established (106–109). Among the complications attending such a calculation are that (*a*) magnetic dipole contributions enter at quadrupole order and (*b*) the molecular response properties one might require as input are not straightforward to obtain from standard quantum chemistry software.

The ability to focus on asymmetric environments, together with the fact that symmetry appears to be broken only within a few angstroms of the air-water interface, makes SFG a promising tool to examine the surprising adsorption behavior of small anions (110–113). Calculations of $\langle u_z \rangle_{\mathcal{E}}$ from simulations with dissolved ions give a sense for how solute-induced spectral changes should be interpreted (101). Whereas Raman shifts in bulk solution are dominated by the very local influence of the ion, predicted SFG changes are predominantly very nonlocal, reflecting symmetry breaking by the ion over large scales.

In bulk water, the reaction field induced by a spherical ion is radially symmetric; according to DCT, the strength of the average induced polarization decays as the inverse square of the distance r from the solute. In this symmetric environment, averaging the (vectorial) polarization over all space yields zero. Placing the solute near an interface with vapor essentially truncates this reaction field at the liquid's boundary, yielding a nonzero average polarization (which we loosely equate here with average molecular orientation). The contribution to this average from the collection of solvent molecules at distance r is determined by the product of induced polarization strength ($\sim r^{-2}$) and the number of molecules at that distance ($\sim r^2$). By this argument, the signal from the collection of directly coordinating molecules will be overwhelmed by that of equally contributing but more numerous collections at larger distances. Indeed, simulations show that changes in $\langle u_z \rangle_{\mathcal{E}}$ induced by monovalent anions of different sizes, whose impacts on solvent are distinct only on small length scales, are nearly identical (101). Similarly, changes due to monovalent cations are indistinguishable from those of anions but in the opposite direction.

Any real macroscopic salt solution will contain both cations and anions. If both are monovalent and are identically distributed in space, then the polarization effects described above should cancel.

However, if their surface propensities differ, then these long-range effects do not cancel, yielding a strong signature of differential adsorption. Because this signal is dominated by solvent molecules well away from a solute, extracting from SFG more detailed information regarding local solvation structure is likely to prove difficult.

7. OUTLOOK

In summarizing the recent theoretical study of aqueous vibrational spectroscopy and the fluctuations it probes, I present my own perspective on a mature and active field, rooted in decades of foundational work. Despite substantial progress and insight, some basic questions remain unanswered, and some technical challenges persist. It is not clear, for example, why simple theories should find detailed success where more elaborate approaches have not. Ongoing developments in interfacing classical and quantum dynamics, as well as high-level quantum chemistry calculations for large water clusters, may prove essential for this purpose. It is also unclear what levels of theory and model realism are needed to capture SFG lineshapes for aqueous interfaces. Recent work has focused on developing molecular mechanics models with extensive input from electronic structure calculations and has successfully reproduced SFG features on the low-frequency edge of the OH stretching band (114, 115). Determining whether such improved energetics are necessary and/or sufficient awaits calculations of the full SFG susceptibility, which in turn await the evaluation of nonstandard molecular response properties from quantum chemistry.

Comprehensive physical pictures of ion solvation at interfaces appear within near-term reach. Predictive theories based on this understanding are likely further off. Some key ingredients are available from theories of capillary waves and hydrophobic solvation at interfaces, as well as classic theories for density and polarization fluctuations in bulk. Combining these mathematical descriptions appropriately, however, involves significant challenges.

Addressing these outstanding issues will enable key physical insights into interfacial systems of intense modern interest. The broad implications for biophysics, catalysis, energy sciences, and materials chemistry should inspire the effort needed to do so.

DISCLOSURE STATEMENT

The author is not aware of any affiliations, memberships, funding, or financial holdings that might be perceived as affecting the objectivity of this review.

ACKNOWLEDGMENTS

This work was supported by the Director, Office of Science, Office of Basic Energy Sciences, Chemical Sciences, Geosciences, and Biosciences Division of the US Department of Energy under contract DE-AC02-05CH11231. I thank Surinarayanan Vaikuntanathan, Andrei Tokmakoff, and especially David Limmer for critical readings of the manuscript. I also thank Nicholas Lewis for processing results of molecular dynamics trajectories to generate the data plotted in **Figure 2**. Jared Smith and Rich Saykally provided the experimental data plotted in **Figure 1**.

LITERATURE CITED

1. Rahman A, Stillinger FH. 1971. Molecular dynamics study of liquid water. *J. Chem. Phys.* 55:3336–59
2. Wernet P, Nordlund D, Bergmann U, Cavalleri M, Odelius M, et al. 2004. The structure of the first coordination shell in liquid water. *Science* 304:995–99

3. Clark GNI, Cappa CD, Smith JD, Saykally RJ, Head-Gordon T. 2010. The structure of ambient water. *Mol. Phys.* 108:1415–33
4. Molinero V, Moore EB. 2009. Water modeled as an intermediate element between carbon and silicon. *J. Phys. Chem. B* 113:4008–16
5. Giovambattista N, Debenedetti PG, Rossky PJ. 2007. Hydration behavior under confinement by nanoscale surfaces with patterned hydrophobicity and hydrophilicity. *J. Phys. Chem. C* 111:1323–32
6. Patel AJ, Varilly P, Chandler D. 2010. Fluctuations of water near extended hydrophobic and hydrophilic surfaces. *J. Phys. Chem. B* 114:1632–37
7. Rasaiah JC, Garde S, Hummer G. 2008. Water in nonpolar confinement: from nanotubes to proteins and beyond. *Annu. Rev. Phys. Chem.* 59:713–40
8. Geissler PL, Chandler D. 2000. Importance sampling and theory of nonequilibrium solvation dynamics in water. *J. Chem. Phys.* 113:9759–65
9. Hummer G, Garde S, Garcia AE, Pohorille A, Pratt LR. 1996. An information theory model of hydrophobic interactions. *Proc. Natl. Acad. Sci. USA* 93:8951–55
10. Pratt LR, Chandler D. 1977. Theory of the hydrophobic effect. *J. Chem. Phys.* 67:3683–704
11. Chandler D. 1993. Gaussian field model of fluids with an application to polymeric fluids. *Phys. Rev. E* 48:2898–905
12. Song XY, Chandler D, Marcus RA. 1996. Gaussian field model of dielectric solvation dynamics. *J. Phys. Chem.* 100:11954–59
13. Lum K, Chandler D, Weeks JD. 1999. Hydrophobicity at small and large length scales. *J. Phys. Chem. B* 103:4570–77
14. Wallqvist A, Berne BJ. 1995. Computer simulation of hydrophobic hydration forces on stacked plates at short range. *J. Phys. Chem.* 99:2893–99
15. Skinner JL, Auer BM, Lin YS. 2009. Vibrational line shapes, spectral diffusion, and hydrogen bonding in liquid water. *Adv. Chem. Phys.* 142:59–103
16. Badger RM. 1940. The relation between the energy of a hydrogen bond and the frequencies of the O-H bands. *J. Chem. Phys.* 8:288–89
17. Nakamoto K, Margoshes M, Rundle RE. 1955. Stretching frequencies as a function of distances in hydrogen bonds. *J. Am. Chem. Soc.* 77:6480–86
18. Novak A. 1974. Hydrogen bonding in solids: correlation of spectroscopic and crystallographic data. In *Structure and Bonding*, ed. JD Dunitz, 18:177–216. New York: Springer-Verlag
19. Green JL, Lacey AR, Sceats MG. 1986. Spectroscopic evidence for spatial correlations of hydrogen bonds in liquid water. *J. Phys. Chem.* 90:3958–64
20. Hare DE, Sorensen CM. 1992. Interoscillator coupling effects on the OH stretching band of liquid water. *J. Chem. Phys.* 96:13–22
21. Falk M, Ford TA. 1966. Infrared spectrum and structure of liquid water. *Can. J. Chem.* 44:1699–707
22. Belch AC, Rice SA. 1983. The OH stretching spectrum of liquid water: a random network model interpretation. *J. Chem. Phys.* 78:4817–23
23. Rice SA, Bergren MS, Belch AC, Nielson G. 1983. A theoretical analysis of the OH stretching spectra of ice Ih, liquid water, and amorphous solid water. *J. Phys. Chem.* 87:4295–308
24. Wall TT, Hornig DF. 1965. Raman intensities of HDO and structure in liquid water. *J. Chem. Phys.* 43:2079–87
25. Auer BM, Skinner JL. 2008. IR and Raman spectra of liquid water: theory and interpretation. *J. Chem. Phys.* 128:224511
26. Mukamel S. 1995. *Principles of Nonlinear Optical Spectroscopy*. New York: Oxford Univ. Press
27. Oxtoby DW, Levesque D, Weis JJ. 1978. Molecular dynamics simulation of dephasing in liquid nitrogen. *J. Chem. Phys.* 68:5528–33
28. Levesque D, Weis JJ, Oxtoby DW. 1980. Molecular dynamics simulation of dephasing in liquid nitrogen. II. Effect of the pair potential on dephasing. *J. Chem. Phys.* 72:2744–49
29. Lawrence CP, Skinner JL. 2002. Vibrational spectroscopy of HOD in liquid D_2O. II. Infrared line shapes and vibrational Stokes shift. *J. Chem. Phys.* 117:8847–54

30. Corcelli SA, Lawrence CP, Skinner JL. 2004. Combined electronic structure/molecular dynamics approach for ultrafast infrared spectroscopy of dilute HOD in liquid H_2O and D_2O. *J. Chem. Phys.* 120:8107–17
31. Stephens MD, Saven JG, Skinner JL. 1997. Molecular theory of electronic spectroscopy in nonpolar fluids: ultrafast solvation dynamics and absorption and emission line shapes. *J. Chem. Phys.* 106:2129–44
32. Saven JG, Skinner JL. 1993. A molecular theory of the line shape: inhomogeneous and homogeneous electronic spectra of dilute chromophores in nonpolar fluids. *J. Chem. Phys.* 99:4391–402
33. Everitt KF, Skinner JL. 2001. Isotropic Raman line shapes of N_2 and O_2 along their liquid-gas coexistence lines. *J. Chem. Phys.* 115:8531–39
34. Corcelli SA, Skinner JL. 2005. Infrared and Raman line shapes of dilute HOD in liquid H_2O and D_2O from 10 to 90°C. *J. Phys. Chem. A* 109:6154–65
35. Auer B, Kumar R, Schmidt JR, Skinner JL. 2007. Hydrogen bonding and Raman, IR, and 2D-IR spectroscopy of dilute HOD in liquid D_2O. *Proc. Natl. Acad. Sci. USA* 104:14215–20
36. Loparo JJ, Roberts ST, Nicodemus RA, Tokmakoff A. 2007. Variation of the transition dipole moment across the OH stretching band of water. *Chem. Phys.* 341:218–29
37. Harder E, Eaves JD, Tokmakoff A, Berne BJ. 2005. Polarizable molecules in the vibrational spectroscopy of water. *Proc. Natl. Acad. Sci. USA* 102:11611–16
38. Paesani F, Xantheas SS, Voth GA. 2009. Infrared spectroscopy and hydrogen-bond dynamics of liquid water from centroid molecular dynamics with an ab initio–based force field. *J. Phys. Chem. B* 113:13118–30
39. Moller KB, Rey R, Hynes JT. 2004. Hydrogen bond dynamics in water and ultrafast infrared spectroscopy: a theoretical study. *J. Phys. Chem. A* 108:1275–89
40. Hayashi T, Jansen TL, Zhuang W, Mukamel S. 2005. Collective solvent coordinates for the infrared spectrum of HOD in D_2O based on an ab initio electrostatic map. *J. Phys. Chem. A* 109:64–82
41. Eaves JD, Tokmakoff A, Geissler PL. 2005. Electric field fluctuations drive vibrational dephasing in water. *J. Phys. Chem. A* 109:9424–36
42. Smith JD, Saykally RJ, Geissler PL. 2007. The effects of dissolved halide anions on hydrogen bonding in liquid water. *J. Am. Chem. Soc.* 129:13847–56
43. Sadlej J, Buch V, Kazimirski JK, Buck U. 1999. Theoretical study of structure and spectra of cage clusters $(H_2O)_n$, $n = 7$–10. *J. Phys. Chem. A* 103:4933–47
44. Kubo R, Toda M, Hashitsume N. 1995. *Statistical Physics II: Nonequilibrium Statistical Mechanics*. Springer Ser. Solid-State Sci. New York: Springer
45. Smith JD, Cappa CD, Wilson KR, Cohen RC, Geissler PL, Saykally RJ. 2005. Unified description of temperature-dependent hydrogen-bond rearrangements in liquid water. *Proc. Natl. Acad. Sci. USA* 102:14171–74
46. Rey R, Moller KB, Hynes JT. 2002. Hydrogen bond dynamics in water and ultrafast infrared spectroscopy. *J. Phys. Chem. A* 106:11993–96
47. Lawrence CP, Skinner JL. 2003. Vibrational spectroscopy of HOD in liquid D_2O. III. Spectral diffusion, and hydrogen-bonding and rotational dynamics. *J. Chem. Phys.* 118:264–72
48. Madden P, Kivelson D. 1984. A consistent molecular treatment of dielectric phenomena. *Adv. Chem. Phys.* 56:467–566
49. Kuharski RA, Bader JS, Chandler D, Sprik M, Klein ML, Impey RW. 1988. Molecular model for aqueous ferrous-ferric electron transfer. *J. Chem. Phys.* 89:3248–57
50. Terpstra P, Combes D, Zwick A. 1990. Effect of salts on dynamics of water: a Raman spectroscopy study. *J. Chem. Phys.* 92:65–70
51. Schultz JW, Hornig DF. 1961. The effect of dissolved alkali halides on the Raman spectrum of water. *J. Phys. Chem.* 65:2131–38
52. Fischer WB, Fedorowicz A, Koll A. 2001. Structured water around ions: FTIR difference spectroscopy and quantum-mechanical calculations. *Phys. Chem. Chem. Phys.* 3:4228–34
53. Walrafen GE. 2005. New Raman method for aqueous solutions: ξ-function dispersion evidence for strong F^--water H-bonds in aqueous CsF and KF solutions. *J. Chem. Phys.* 123:074506
54. Nickolov ZS, Miller JD. 2005. Water structure in aqueous solutions of alkali halide salts: FTIR spectroscopy of the OD stretching band. *J. Colloid Interface Sci.* 287:572–80

55. Dillon SR, Dougherty RC. 2002. Raman studies of the solution structure of univalent electrolytes in water. *J. Phys. Chem. A* 106:7647–50
56. Senior WA, Verrall RE. 1969. Spectroscopic evidence for the mixture model in HOD solutions. *J. Phys. Chem.* 73:4242–49
57. D'Arrigo G, Maisano G, Mallamace F, Migliardo P, Wanderlingh F. 1981. Raman scattering and structure of normal and supercooled water. *J. Chem. Phys.* 75:4264–70
58. Walrafen GE, Hokmabadi MS, Yang WH. 1986. Raman isosbestic points from liquid water. *J. Chem. Phys.* 85:6964–69
59. Hare DE, Sorensen CM. 1990. Raman spectroscopic study of dilute HOD in liquid H_2O in the temperature range −31.5 to 160°C. *J. Chem. Phys.* 93:6954–61
60. Geissler PL. 2005. Temperature dependence of inhomogeneous broadening: on the meaning of isosbestic points. *J. Am. Chem. Soc.* 127:14930–35
61. Fecko CJ, Eaves JD, Loparo JJ, Tokmakoff A, Geissler PL. 2003. Ultrafast hydrogen-bond dynamics in the infrared spectroscopy of water. *Science* 301:1698–702
62. Asbury JB, Steinel T, Kwak K, Corcelli SA, Lawrence CP, et al. 2004. Dynamics of water probed with vibrational echo correlation spectroscopy. *J. Chem. Phys.* 121:12431–46
63. Asbury JB, Steinel T, Stromberg C, Corcelli SA, Lawrence CP, et al. 2004. Water dynamics: vibrational echo correlation spectroscopy and comparison to molecular dynamics simulations. *J. Phys. Chem. A* 108:1107–19
64. Nibbering ETJ, Elsaesser T. 2004. Ultrafast vibrational dynamics of hydrogen bonds in the condensed phase. *Chem. Rev.* 104:1887–914
65. Steinel T, Asbury JB, Corcelli SA, Lawrence CP, Skinner JL, Fayer MD. 2004. Water dynamics: dependence on local structure probed with vibrational echo correlation spectroscopy. *Chem. Phys. Lett.* 386:295–300
66. Eaves JD, Loparo JJ, Fecko CJ, Roberts ST, Tokmakoff A, Geissler PL. 2005. Hydrogen bonds in liquid water are broken only fleetingly. *Proc. Natl. Acad. Sci. USA* 102:13019–22
67. Hamm P. 2006. Three-dimensional-IR spectroscopy: beyond the two-point frequency fluctuation correlation function. *J. Chem. Phys.* 124:124506
68. Loparo JJ, Roberts ST, Tokmakoff A. 2006. Multidimensional infrared spectroscopy of water. I. Vibrational dynamics in two-dimensional IR line shapes. *J. Chem. Phys.* 125:194521
69. Loring RF, Mukamel S. 1985. Unified theory of photon echoes: the passage from inhomogeneous to homogeneous line broadening. *Chem. Phys. Lett.* 114:426–29
70. Suarez A, Silbey R. 1994. Low-temperature dynamics in glasses and the stochastic sudden-jump model. *Chem. Phys. Lett.* 218:445–53
71. Everitt KF, Geva E, Skinner JL. 2001. Determining the solvation correlation function from three-pulse photon echoes in liquids. *J. Chem. Phys.* 114:1326–35
72. Piryatinski A, Lawrence CP, Skinner JL. 2003. Vibrational spectroscopy of HOD in liquid D_2O. V. Infrared three-pulse photon echoes. *J. Chem. Phys.* 118:9672–79
73. Hirata F, Rossky PJ. 1981. A realization of "V structure" in liquid water. *J. Chem. Phys.* 74:6867–74
74. Stillinger FH. 1973. Structure in aqueous solutions of nonpolar solutes from the standpoint of scaled-particle theory. *J. Solut. Chem.* 2:141–58
75. Sokhan VP, Tildesley DJ. 1997. The free surface of water: molecular orientation, surface potential and nonlinear susceptibility. *Mol. Phys.* 92:625–40
76. Noah-Vanhoucke J, Smith JD, Geissler PL. 2009. Toward a simple molecular understanding of sum frequency generation at air-water interfaces. *J. Phys. Chem. B* 113:4065–74
77. Petersen PB, Saykally RJ. 2006. On the nature of ions at the liquid water surface. *Annu. Rev. Phys. Chem.* 57:333–64
78. Jungwirth P, Tobias DJ. 2006. Specific ion effects at the air/water interface. *Chem. Rev.* 106:1259–81
79. Jungwirth P, Tobias DJ. 2002. Ions at the air/water interface. *J. Phys. Chem. B* 106:6361–73
80. Jackson JD. 1999. *Classical Electrodynamics*. New York: Wiley. 3rd ed.
81. Onsager L, Samaras NNT. 1934. The surface tension of Debye-Hückel electrolytes. *J. Chem. Phys.* 2:528–36

82. Markin VS, Volkov AG. 2002. Quantitative theory of surface tension and surface potential of aqueous solutions of electrolytes. *J. Phys. Chem. B* 106:11810–17
83. Lynden-Bell RM, Rasaiah JC. 1997. From hydrophobic to hydrophilic behaviour: a simulation study of solvation entropy and free energy of simple solutes. *J. Chem. Phys.* 107:1981–91
84. Huang DM, Geissler PL, Chandler D. 2001. Scaling of hydrophobic solvation free energies. *J. Phys. Chem. B* 105:6704–9
85. Caleman C, Hub JS, van Maaren PJ, van der Spoel D. 2011. Atomistic simulation of ion solvation in water explains surface preference of halides. *Proc. Natl. Acad. Sci. USA* 108:6838–42
86. Otten DE, Shaffer PR, Geissler PL, Saykally RJ. 2012. Elucidating the mechanism of selective ion adsorption to the liquid water surface. *Proc. Natl. Acad. Sci. USA* 109:701–5
87. Levin Y. 2009. Polarizable ions at interfaces. *Phys. Rev. Lett.* 102:147803
88. Levin Y, dos Santos AP, Diehl A. 2009. Ions at the air-water interface: an end to a hundred-year-old mystery? *Phys. Rev. Lett.* 103:257802
89. Noah-Vanhoucke J, Geissler PL. 2009. On the fluctuations that drive small ions toward, and away from, interfaces between polar liquids and their vapors. *Proc. Natl. Acad. Sci. USA* 106:15125–30
90. Song XY, Chandler D. 1998. Dielectric solvation dynamics of molecules of arbitrary shape and charge distribution. *J. Chem. Phys.* 108:2594–600
91. Weeks JD. 1977. Structure and thermodynamics of the liquid-vapor interface. *J. Chem. Phys.* 67:3106–21
92. Vaikuntanathan S, Shaffer PR, Geissler PL. 2013. Adsorption of solutes at liquid-vapor interfaces: insights from lattice gas models. *Faraday Discuss.* 160:63–74
93. Zhu XD, Suhr H, Shen YR. 1987. Surface vibrational spectroscopy by infrared-visible sum frequency generation. *Phys. Rev. B* 35:3047–50
94. Du Q, Superfine R, Freysz E, Shen YR. 1993. Vibrational spectroscopy of water at the vapor/water interface. *Phys. Rev. Lett.* 70:2313–16
95. Shen YR, Ostroverkhov V. 2006. Sum-frequency vibrational spectroscopy on water interfaces: polar orientation of water molecules at interfaces. *Chem. Rev.* 106:1140–54
96. Walker DS, Richmond GL. 2007. Understanding the effects of hydrogen bonding at the vapor-water interface: vibrational sum frequency spectroscopy of H_2O/HOD/D_2O mixtures studied using molecular dynamics simulations. *J. Phys. Chem. C* 111:8321–30
97. Sovago M, Campen RK, Wurpel GWH, Muller M, Bakker HJ, Bonn M. 2008. Vibrational response of hydrogen-bonded interfacial water is dominated by intramolecular coupling. *Phys. Rev. Lett.* 100:173901
98. Nihonyanagi S, Ishiyama T, Lee T, Yamaguchi S, Bonn M, et al. 2011. Unified molecular view of the air/water interface based on experimental and theoretical $\chi^{(2)}$ spectra of an isotopically diluted water surface. *J. Am. Chem. Soc.* 133:16875–80
99. Morita A, Hynes JT. 2000. A theoretical analysis of the sum frequency generation spectrum of the water surface. *Chem. Phys.* 258:371–90
100. Morita A, Hynes JT. 2002. A theoretical analysis of the sum frequency generation spectrum of the water surface. II. Time-dependent approach. *J. Phys. Chem. B* 106:673–85
101. Noah-Vanhoucke J, Smith JD, Geissler PL. 2009. Statistical mechanics of sum frequency generation spectroscopy for the liquid-vapor interface of dilute aqueous salt solutions. *Chem. Phys. Lett.* 470:21–27
102. Auer BM, Skinner JL. 2008. Vibrational sum-frequency spectroscopy of the liquid/vapor interface for dilute HOD in D_2O. *J. Chem. Phys.* 129:214705
103. Tian CS, Shen YR. 2009. Isotopic dilution study of the water/vapor interface by phase-sensitive sum-frequency vibrational spectroscopy. *J. Am. Chem. Soc.* 131:2790–91
104. Byrnes SJ, Geissler PL, Shen YR. 2011. Ambiguities in surface nonlinear spectroscopy calculations. *Chem. Phys. Lett.* 516:115–24
105. Shen YR. 1999. Surface contribution versus bulk contribution in surface nonlinear optical spectroscopy. *Appl. Phys. B* 68:295–300
106. Morita A. 2004. Toward computation of bulk quadrupolar signals in vibrational sum frequency generation spectroscopy. *Chem. Phys. Lett.* 398:361–66
107. Neipert C, Space B, Roney AB. 2007. Generalized computational time correlation function approach: quantifying quadrupole contributions to vibrationally resonant second-order interface-specific optical spectroscopies. *J. Phys. Chem. C* 111:8749–56

108. Munn RW. 1996. A general microscopic theory of bulk second-harmonic generation from molecular crystals. *Mol. Phys.* 89:555–69
109. Zhu XD, Wong A. 1992. Multipolar contributions to coherent optical second-harmonic generation at an interface between two isotropic media: a quantum-electrodynamic calculation. *Phys. Rev. B* 46:2540–44
110. Jubb AM, Hua W, Allen HC. 2012. Organization of water and atmospherically relevant ions and solutes: vibrational sum frequency spectroscopy at the vapor/liquid and liquid/solid interfaces. *Acc. Chem. Res.* 45:110–19
111. Hopkins AJ, Schrodle S, Richmond GL. 2010. Specific ion effects of salt solutions at the CaF_2/water interface. *Langmuir* 26:10784–90
112. Tian CS, Byrnes SJ, Han HL, Shen YR. 2011. Surface propensities of atmospherically relevant ions in salt solutions revealed by phase-sensitive sum frequency vibrational spectroscopy. *J. Phys. Chem. Lett.* 2:1946–49
113. Imamura T, Mizukoshi Y, Ishiyama T, Morita A. 2012. Surface structures of NaF and Na_2SO_4 aqueous solutions: specific effects of hard ions on surface vibrational spectra. *J. Phys. Chem. C* 116:11082–90
114. Ishiyama T, Morita A. 2009. Analysis of anisotropic local field in sum frequency generation spectroscopy with the charge response kernel water model. *J. Chem. Phys.* 131:244714
115. Pieniazek PA, Tainter CJ, Skinner JL. 2011. Interpretation of the water surface vibrational sum-frequency spectrum. *J. Chem. Phys.* 135:044701

Annual Review of
Physical Chemistry
Volume 64, 2013

Contents

Indexes

Errata

An online log of corrections to *Annual Review of Physical Chemistry* articles may be found at http://physchem.annualreviews.org/errata.shtml